Hindawi
Journal of Nanomaterials
Volume 2017, Article ID 4604159, 9 pages
https://doi.org/10.1155/2017/4604159

Research Article

Continuous Synthesis of Ag/TiO_2 Nanoparticles with Enhanced Photocatalytic Activity by Pulsed Laser Ablation

Rui Zhou,[1] Shengdong Lin,[1] Huixin Zong,[2] Tingting Huang,[1] Fengping Li,[1,3] Jiahong Pan,[2] and Jingqin Cui[4]

[1] *School of Aerospace Engineering, Xiamen University, Xiamen, Fujian Province 361005, China*
[2] *Renewable Energy School, North China Electric Power University, Beijing 102206, China*
[3] *Zhejiang Provincial Key Laboratory of Laser Processing Robot/Key Laboratory of Laser Precision Processing & Detection, Wenzhou University, Wenzhou, Zhejiang Province 325035, China*
[4] *Pen-Tung Sah Institute of Micro-Nano Science and Technology, Xiamen University, Xiamen, Fujian Province 361005, China*

Correspondence should be addressed to Rui Zhou; rzhou2@xmu.edu.cn

Received 5 August 2017; Revised 25 September 2017; Accepted 10 October 2017; Published 16 November 2017

Academic Editor: Takuya Tsuzuki

A facile and environmental friendly synthesis strategy based on pulsed laser ablation has been developed for potential mass production of Ag-loaded TiO_2 (Ag/TiO_2) nanoparticles. By sequentially irradiating titanium and silver target substrates, respectively, with the same 1064 nm 100 ns fiber laser, Ag/TiO_2 particles can be fabricated. A postannealing process leads to the crystallization of TiO_2 to anatase phase with high photocatalytic activity. The phase composition, microstructure, and surface state of the elaborated Ag/TiO_2 are characterized by X-ray diffraction (XRD), energy dispersive X-ray (EDX), field emission scanning electron microscope (FESEM), transmission electron microscope (TEM), and X-ray photoelectron spectroscopy (XPS) techniques. The results suggest that the presence of silver clusters deposited on the surface of TiO_2 nanoparticles. The nanostructure is formed through laser interaction with materials. Photocatalytic activity evaluation shows that silver clusters could significantly enhance the photocatalytic activity of TiO_2 in degradation of methylene blue (MB) under UV light irradiation, which is attributed to the efficient electron traps by Ag clusters. Our developed Ag/TiO_2 nanoparticles synthesized via a straightforward, continuous, and green pathway could have great potential applications in photocatalysis.

1. Introduction

Due to highly rigid demanding for various functional photocatalysts in environmental applications, TiO_2 stands as one of the most widely studied semiconductors and highlighted for heterogeneous photocatalysts [1–3]. By splitting water in solar energy conversion cells, it also serves as the promising candidate for photoanode material. The distinguished popularity of TiO_2 is attributed to many advantages, such as relatively high quantum efficiency, low cost, biocompatibility, and high optical and chemical stability [4–6]. However, two obvious shortcomings restrain the wide applications of TiO_2. On the one hand, the rapid electron-hole recombination results in low quantum yield, which makes it more difficult to efficiently purify sewage in large scale and concentrated pollutants [7]. On the other hand, limited by its wide band gap (~3.2 eV), TiO_2 can only take effect in the UV region of the solar spectrum (~5% of the solar energy), while the energy absorption in the range of visible light containing about 45% of the solar energy [8] cannot be captured. In order to extend the spectral range of the TiO_2 response, various methods have been proposed, such as coupling with metals or narrow band gap semiconductors, doping, and surface sensitization by organic dyes [9–11]. However, there are some unavoidable defects in these methods. For example, the preparation method of metal doping is complex [12] and photosensitizer could be easily degraded, making photocatalyst unstable [13].

Deposition of noble metals, such as Ag and Au, on TiO_2 serves as one of the effective methods to reduce the chance of electron-hole recombination in photocatalytic process. With the versatile properties of photocatalytic and antibactericidal activities [14, 15], Ag is widely coupled with TiO_2. In this

system, Ag could contribute to the formation of Schottky barriers at Ag/TiO_2 interfacial contact area, resulting in the reduction of electron-hole recombination in the photocatalytic process [16]. Meanwhile, silver brings in extra absorption bands at visible light spectra due to surface plasmon resonance (SPR) effect [17, 18]. The spectral range of the response of TiO_2 could be further extended to a much longer wavelength.

In recent years, novel Ag-containing photocatalysts have been prepared by developing various technologies and their activities were investigated [19, 20]. Controlling the structural parameters of Ag is of particular importance which determines the efficiency and physicochemical properties of the resultant photocatalysts. For instance, photoreduction method has already been conventionally used by several research groups [21, 22]. However, it is found that the photocatalytic activity of Ag/TiO_2 could not be obviously enhanced compared to that of TiO_2. Also, the controllability of deposition of Ag on TiO_2 surface is weak in the process. As the regular methods, photodeposition, chemical reduction, and thermal impregnation usually require complicated equipment or toxic nitrogen for modification of TiO_2 with Ag [21, 23, 24]. Hence, it is desired to explore a simple and nontoxic method to fabricate Ag/TiO_2 composite nanoparticles. As known, laser ablation is considered as a flexible method to synthesize nanoparticles, and thus a few elaborated carbon nanoparticles, ultrafine TiO_2 nanoparticles, and silicon nanoparticles have been reported [25–27]. Compared with conventional nanoparticles synthesized via wet chemical route, laser ablation offers an alternative green route to well-separated nanoparticles.

In this paper, an easily hand-on and straightforward approach is presented by employing the pulsed laser ablation in water to fabricate Ag deposited TiO_2 particles. A two-step process is developed by the combination of laser ablation of different targeted substrates. Scanning electron microscope (SEM), transmission electron microscope (TEM), energy dispersive X-ray (EDX), X-ray photoelectron spectroscopy (XPS), and X-ray diffraction (XRD) are performed to characterize the properties of Ag/TiO_2 nanoparticles. To our best knowledge, this is the first time to employ laser to continuously fabricate Ag/TiO_2 composite nanoparticles which are used in photocatalytic degradation successfully.

2. Experimental

2.1. Materials. A silver plate (99.8% in purity) with dimensions of Φ15 mm (diameter) × 2 mm (thickness) and a titanium plate (99.99% in purity) with dimensions of 20 mm (length) × 20 mm (width) × 2 mm (thickness) were purchased as targeted metal substrates. All the targeted substrates were alternatively washed in DI water and ethanol for several times. Each substrate was ultrasonicated for 30 mins in DI water and then ethanol separately before laser processing.

2.2. Production of Nanoparticles. The experimental setup of laser ablation is shown in Figure 1. The synthesis of TiO_2 nanoparticles was performed using a 1064 nm 100 ns fiber laser ablation. A titanium metal plate (10 mm) was fixed on

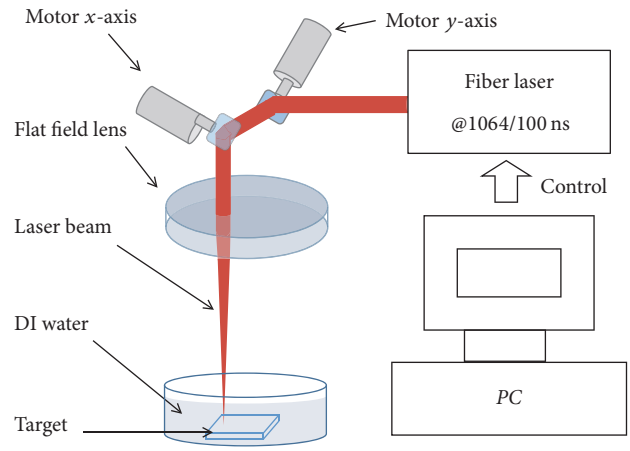

Figure 1: Experimental setup for fabricating nanoparticles by laser ablation.

the bottom of a glass vessel filled with 3.5 cm^3 DI water and the level of water/air interface above the targeted substrate was about 2 mm in height. The metal plate was irradiated through focusing a lens with focal length of 329 mm, and it should be noted that the thickness of water level above the substrate was taken into account regarding the laser beam focal length. The spot size incident upon the targeted metal plate surface was focused to approximately 0.05 mm in diameter. The pulsed laser power was 2.43 W, the repetition rate was 20 kHz, and the fluence was about 6.11 J/cm^2. As the irradiation of the metal surface results in fast removal of materials confined in the laser spot, the laser beam scanning system via x-y galvo scanners was employed to ensure that the ablation occurred on a fresh spot to avoid the formation of deep holes. The laser scanning speed was typically fixed at 1000 mm/s. The ablation area on the sample surface was 10 mm × 10 mm. The titanium plate was taken out of the vessel after the laser ablation for 10 mins, and the silver plates were subsequently put into the TiO_2 nanoparticle solution. Meanwhile, the laser power and repetition rate were changed to 3.9 W and 60 kHz accordingly with the other remaining parameters unchanged. Ag/TiO_2 nanoparticles were synthesized under defined laser processing conditions. The nanoparticles were isolated, dried, and fully crystallized by annealing at 450°C for 2 h.

2.3. Material Characterization. The characterization of as-prepared TiO_2 and Ag/TiO_2 particles was performed by field emission scanning electron microscope (FESEM), transmission electron microscope (TEM), energy dispersive X-ray detector (EDX), X-ray photoelectron spectroscopy (XPS), and X-ray diffraction (XRD).

The size and morphology were characterized by FESEM (SU-70) and TEM (JEM-1400). For FESEM, a drop of solution was deposited onto a silicon wafer; then the substrate was allowed to dry at 60°C by a drying oven. A microgrid copper mesh (carbon on 400 copper mesh) was used, and the solution was dropped onto the mesh and dried at room temperature. The lattice structures of the as-prepared samples were studied by XRD (D8.ADVANCE) with a 2θ step size

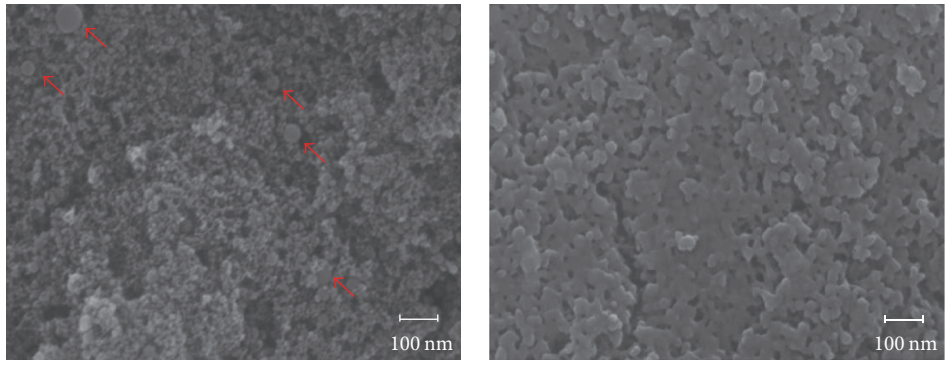

(a) (b)

Figure 2: FESEM images of as-synthesized TiO_2 nanoparticles (a) and Ag/TiO_2 nanoparticles (b) generated by laser ablation in water.

of 0.02. XPS analyses were performed using Thermo Fisher K-Alpha. An incident monochromated X-ray beam from the Al$K\alpha$ target (12 kV, 4.2 mA) was focused on a 0.3 mm × 0.3 mm area of the sample surface with a sputter rate of 0.28 nm/s. The electron energy analyzer was operated with a pass energy of 50 eV enabling high resolution of the spectra to be obtained.

2.4. Photocatalytic Activity. The photocatalytic activity was evaluated by the photodegradation of 1.0 mg/L of methylene blue (MB) with LED light source with the wavelength of 365 nm in Perfectlight multichannel photocatalytic reaction system (PCX50A). The concentration of photocatalyst was fixed at 1.0 g/L. After irradiation for 2 h, the liquid sample was collected by membrane filtration (pore size: ~0.2 μm). UV-Vis spectrophotometer (Shimadzu UV-1700) was employed to measure the concentration of methylene blue in the wavelength range of 663 nm to confirm the photocatalytic degradation efficiency.

3. Results and Discussion

3.1. Morphology and Particle Size. The morphology and size distribution of Ag/TiO_2 nanoparticles were observed by FESEM. For comparison, a part of TiO_2 nanoparticles was collected for characterizations before laser ablation of Ag metal plate. As shown in Figure 2, the morphology of nanoparticles revealed by FESEM shows a significant difference between the pure TiO_2 and Ag/TiO_2. While both two samples show well-densified structures, the morphology of constituted nanoparticles seems to be different. It could be seen that the pure TiO_2 shows a granular structure with the average size of approximately 5~15 nm in diameter. The presence of agglomerations of spherical nanoparticles with the sizes of about 20–80 nm is also observed as indicated by the red arrows in Figure 2(a). By contrast, the Ag/TiO_2 nanoparticles show a completely different morphology in Figure 2(b). The surface of Ag/TiO_2 is much smoother than that of pure TiO_2, while plenty of larger particles together with a granular structure indicated the presence of mixed phases, which could be further revealed by the XRD results of the corresponding powders. Based on the previous reported research of TiO_2 particle size influence on its photoactivity [28, 29], the effect of particle size plays an important role in TiO_2 photocatalysis, mostly through affecting the dynamics of electron-hole recombination. The photocatalytic activity of TiO_2 could be enhanced as decreasing the particle size of TiO_2, especially to less than 30 nm [29]. It indicates that the TiO_2 nanoparticles fabricated by laser ablation are quite suitable for photocatalytic applications in consideration of size and size distribution.

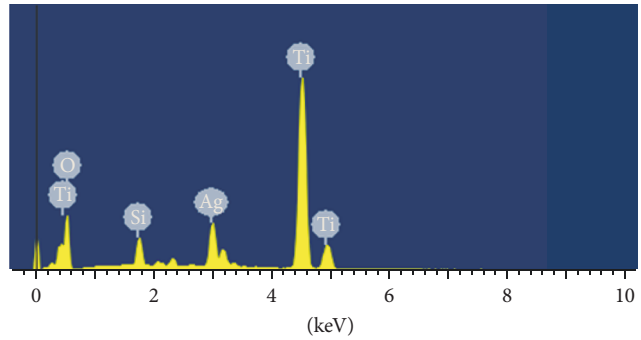

Figure 3: EDX spectrum of the Ag/TiO_2 nanoparticles.

It is also observed that the colors of TiO_2 and Ag/TiO_2 are both grey. The reason may be the formation of the disorder and a little Ti^{3+} species on the surface [30].

The chemical compositions of laser ablated Ag/TiO_2 nanoparticles were determined by energy dispersive X-ray spectroscopy (EDX), which were carried out together with the SEM. As shown in Figure 3, peaks associated with Ti, O, Ag, and Si are clearly observed in the spectrum. The Ti and O peaks confirmed the presence of TiO_2 particles, and Ag peak obviously resulted from Ag nanoparticles. The signal of Si should be attributed to the building element of the substrate since no other Si-based chemicals were used throughout the synthesis. EDX result confirms the existence of Ag nanoparticles.

In most cases, laser ablation in liquid is carried out with a high-power pulsed laser, which could excite free electrons of material surface on the substrate. It is deemed that the excitation energy could be dissipated into heat within a short time. When the laser-induced heat on the substrate surface is still below the vaporization threshold of materials, the laser beam could lead to a fast temperature rise on the surface as the source of heat treatment [31]. The temperature distribution is determined by thermal and optical properties of materials, as well as laser processing parameters. While the laser intensity reaches a certain level leading to significant material vaporization, both the vaporization and melting could arise up on the metal surface. Attributed to Gaussian distribution of the laser beam at the focus point, the energy density at the border of the laser beam is lower than that of the central part, where the surrounding area of laser ablation absorbs less energy. As a result, vapor plume above the material surface can be formed in the central area of laser irradiation with higher temperature. Then the vapor plume may react with water and then be cooled down, leading to the formation of nanoparticles, such as TiO_2 nanoparticles in this case [32, 33]. In the meantime, melting happens under the surrounding area, where the heating temperature is not high enough to vaporize the metal. Subsequently, the molten metal is blown away by high-intensity shock waves by laser plasma, resulting in larger nanoparticles. It explains the observation of parts of large particles in Figure 2(a) combined with the mechanism of Ostwald ripening phenomena [34]. The formation of Ag/TiO_2 is more complicated than that of TiO_2 attributed to the following mechanisms. (i) The thermodynamic state with high temperature, high pressure, and high density of the vapor plume provides a good opportunity to the high-temperature reactions between the Ag vapor plume and the TiO_2 nanoparticles in the liquid; subsequently, the Ag/TiO_2 nanoparticles will be generated. This reaction occurs at the interface between the Ag vapor plume and the liquid. (ii) There may be the other reaction occurring inside the liquid. The extremely high pressure in front of the Ag vapor plume will impinge the ablation species from the Ag target at the plume-liquid interface into the liquid. Subsequently, the reaction between the Ag and TiO_2 occurs inside the liquid, and then Ag/TiO_2 nanoparticles are generated. (iii) Ag nanoparticles with large momentum impinging on titania particles may also generate Ag/TiO_2 nanoparticles.

TEM is employed to further distinguish the difference between TiO_2 nanoparticles and Ag/TiO_2 nanoparticles. In Figure 4(a), it could be seen that the TiO_2 nanoparticles are bright and spherical with the size of most particles ranging from 5 to 15 nm, regardless of aggregated large particles. In Figure 4(b), there are plenty of nanoparticles about 20 nm in size. It is observed that some dark and smaller nanoparticles appear besides existence of similar particles as shown by red arrows in Figure 4(a). As TiO_2 nanoparticles in both samples were prepared under the same experimental conditions, the relatively dark and smaller particles should be silver nanoparticles generated in the second process. It is obvious that most of Ag nanoparticles are firmly attached to TiO_2 nanoparticles closely with very few appearing alone or self-aggregating with each other. It illustrates that Ag/TiO_2 composite nanoparticles were successfully fabricated by laser ablation without doping Ag into TiO_2 particles. As previously mentioned, the particle size's influence on the photoactivity of TiO_2 in water for photooxidation reactions is significant, especially as effective particle sizes are less than 30 nm. It implies that the size of generated TiO_2 particles meets the demand of potential photocatalytic applications.

3.2. Surface Chemistry Analysis. Although EDX probing is effective in element analysis, it cannot differentiate the valence of element. In this occasion, XPS was employed to elucidate the valence of O, Ag, and Ti, to further confirm the existence of Ag. In order to compensate for sample charging, binding energies were referred to that of the adventitious carbon 1 s peak at 285.0 eV [24]. Figure 5(a) shows a strong O 1s peak coupled with a small shoulder observed, and, when fitted, resulting in giving an intense peak centered at 530.4 eV and a small peak at 532.7 eV. The spectra at 530.4 eV can be assigned to oxygen bound to Ti^{4+} (TiO_2) ions in TiO_2, while the spectra at 532.7 eV should be attributed to the existence of hydroxide OH group [35]. The result indicates that some H_2O reacts with TiO_2 and forms Ti-O in the course of laser ablation, such as H_2O + Ti-O-Ti → 2Ti-OH [36]. The predicted Ti^{3+} is not found, possibly due to the low content. In Figure 5(b), the Ag 3d spectra consists of two peaks located at 367.8 eV and 374.2 eV which confirms the presence of the Ag nanoparticles. The Ag $3d_{5/2}$ peak appears at a binding energy of 367.8 eV, which indicates that the silver is in metallic nature. The 6.4 eV difference between the binding energy of Ag $3d_{5/2}$ and $3d_{3/2}$ peaks is also characteristic of metallic Ag 3d states. Figure 5(c) shows the high resolution XPS spectra of the Ti 2p. The binding energies of Ti $2p_{3/2}$ and Ti $2p_{1/2}$ are 458.9 eV and 464.3 eV, respectively. These two peaks are assigned to Ti^{4+} (TiO_2) [36]. It shows that the samples fabricated by laser ablation in water are Ag/TiO_2 nanoparticles.

3.3. XRD Patterns. Figure 6 shows the XRD patterns of different TiO_2-based nanoparticles in the range of diffraction angles 2θ between 20° and 80°. Figure 6(a) shows the XRD pattern of pure rutile (commercial) for photocatalysis as reference, which is used to be compared with as-prepared TiO_2 and Ag/TiO_2. Figures 6(b) and 6(c) show the XRD patterns of pure TiO_2 and Ag/TiO_2 fabricated by pulsed laser ablation followed by annealing under 450°C for 2 h in argon gas, respectively. It is deemed that TiO_2 mostly exists in two main crystal phases, saying rutile and anatase [37]. It can be seen that pure TiO_2 consists of larger portion of anatase, which has been demonstrated to be the most photocatalytically active, and a small amount of rutile. We took the XRD peaks at 25.3° (A101) and 27.4° (R110) as the characteristic peaks of anatase and rutile crystal phase, respectively [38]. Ag/TiO_2 also has a similar XRD pattern to that of pure TiO_2 except a distinguished point. The intensity of rutile peaks increases, while the intensity of anatase peaks slightly decreases, indicating that the crystallization of anatase and rutile was both affected by the deposited Ag nanoparticles. The approximate mass percentage of anatase crystal phase of the samples can be roughly calculated from the following equation as proposed [39, 40]:

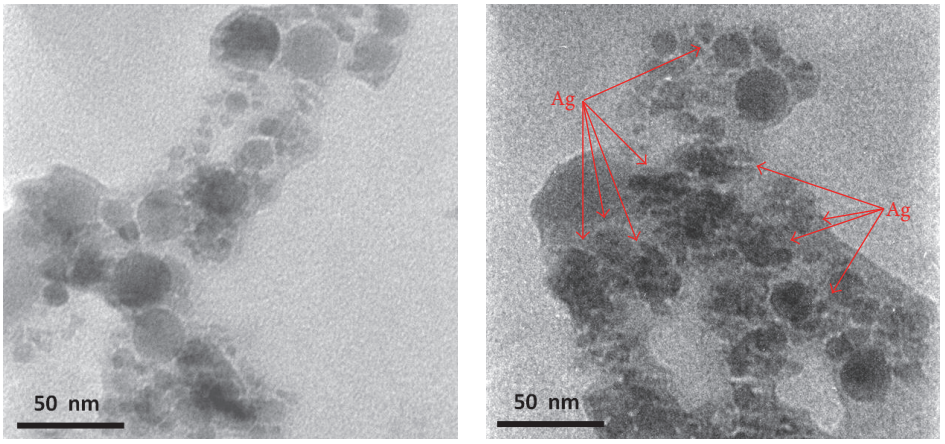

(a) (b)

FIGURE 4: TEM images of (a) TiO_2 nanoparticles and (b) Ag/TiO_2 nanoparticles generated by laser ablation in water. Ag particles were highlighted by red arrows. Scale bar is 50 nm.

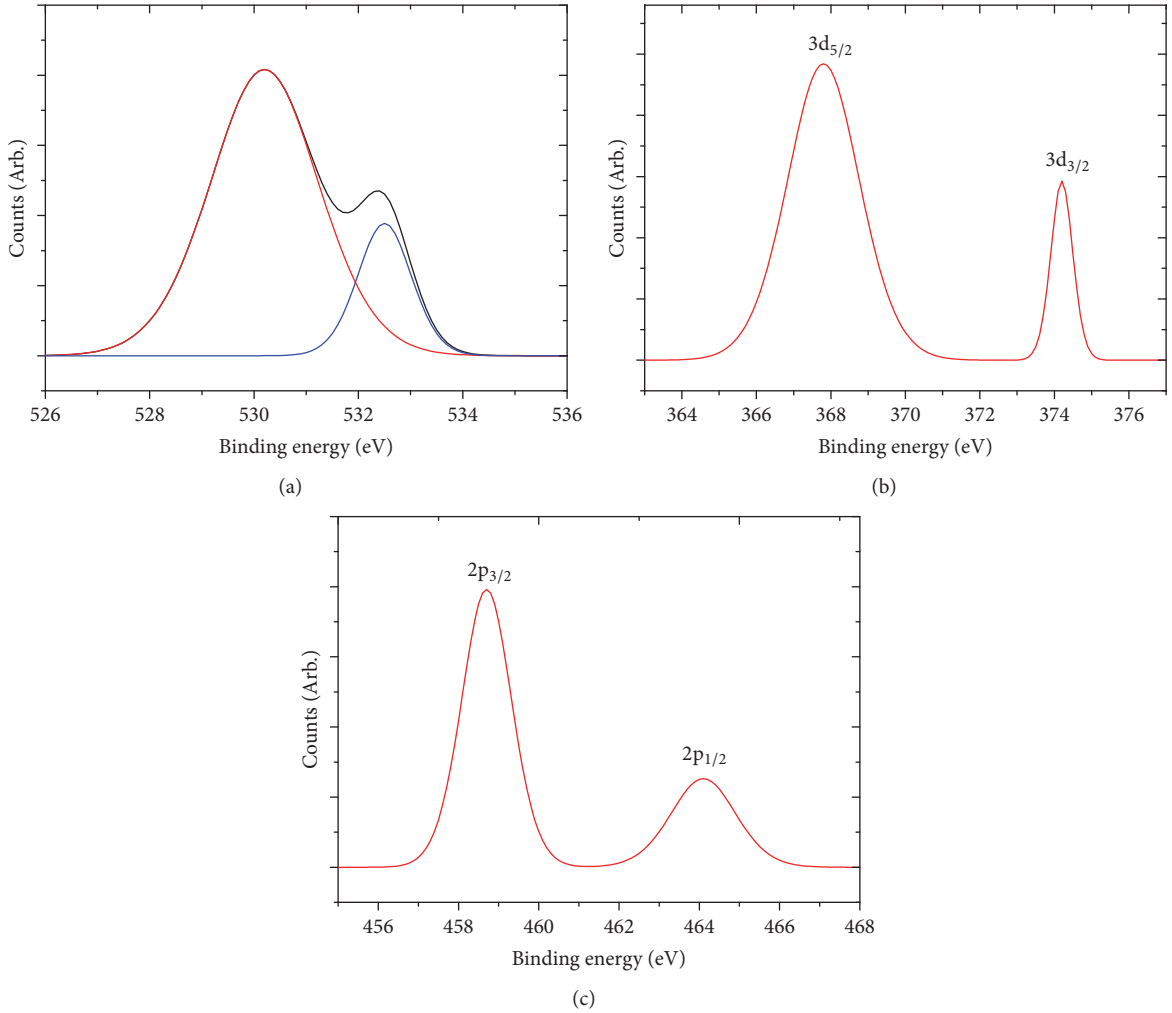

FIGURE 5: XPS images of the Ag/TiO_2 nanoparticles. Peak-fitting spectra at high resolution of (a) O 1s, (b) Ag 3d, and (c) Ti 2p spectra of the Ag/TiO_2 nanoparticles.

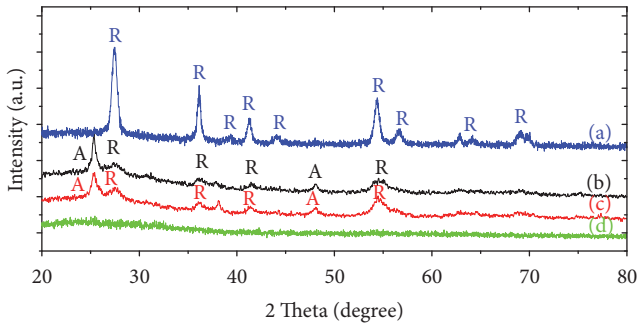

A: anatase
R: rutile

FIGURE 6: X-ray diffraction patterns of TiO_2 powder: (a) rutile; (b) pure TiO_2; (c) Ag/TiO_2; and (d) TiO_2 (before annealing).

$$X_A = \left[1 + 1.26\left(\frac{I_R}{I_A}\right)\right]^{-1}, \quad (1)$$

where X_A is the weight fraction of anatase in the sample. I_A and I_R are the areas of anatase (101) and rutile (110) diffractions, respectively. X_A of Ag/TiO_2 is 76.34% which is lower than 83.24% of pure TiO_2. The reason to explain the decreasing weight fraction of anatase is that the silver nanoparticle accepts electrons from TiO_2, making it charged. In order to achieve the balance of charge, oxygen vacancies appear on the anatase surface, which is beneficial to the atomic rearrangement and restructuring of rutile crystal phase, eventually prompting a phase transformation from anatase to rutile. However, Ag/TiO_2 shows a broader peak width than pure TiO_2, suggesting that Ag hinders the crystal growth of TiO_2. This result is well in agreement with the results from TEM observations.

It is well known that the crystalline structure plays a critical role in catalytic activity for heterogeneous photocatalysts. Because of the difference in Fermi levels of anatase and rutile, the holes and electrons can be efficiently separated through charge carrier transfer. Hence, the mixed phase in TiO_2 may benefit the photocatalytic activity due to the reduced recombination between the excited electrons and holes, as found in the widely studied commercial Aeroxide P-25 TiO_2 [41].

Because particle size plays an important role in the photoactivity, the particle sizes of TiO_2 and Ag/TiO_2 are determined. The average size (D in nm) can be estimated from XRD patterns by the Scherrer formula:

$$D = \frac{k\lambda}{\beta \cos\theta}, \quad (2)$$

where k is a constant equal to 0.89, λ is the X-ray wavelength equal to 0.154 nm, β is the full width at half the maximum, and θ is half the diffraction angle. The calculated results of pure TiO_2 and Ag/TiO_2 are 15.0 and 19.4 nm, respectively, which are consistent with FESEM and TEM results.

Without annealing, the pure TiO_2 is amorphous as the green line shown in Figure 6(d). The mechanism regarding the formation of TiO_2 could be deduced from the reaction

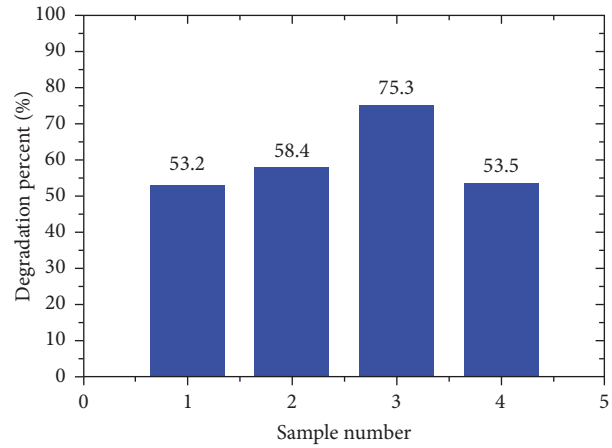

FIGURE 7: Comparison of the methylene blue degradation percent in 1: TiO_2; 2: $Ag/TiO_2{}'$; 3: Ag/TiO_2; and 4: rutile.

dynamics of laser ablation at water-titanium interface. As the laser fluence is high, the induced high-temperature plasma excites, ionizes, and dissociates the surrounding water molecules. The nucleation process of TiO_2 is initiated directly at water-plasma interface, making the formation of crystal phase feasible. The high density of plasma also enhances the molecular reaction rate, increasing the particle size. When the laser fluence is low, the breakdown of water molecules does not effectively take place, leading to insufficiently oxidized nanoparticles of titanium. In order to fabricate the nanoparticles with smaller size, the lower laser fluence was employed in this work. Subsequently, the pure TiO_2 and Ag/TiO_2 were annealed under 450°C for 2 h in the argon air. As can be seen in Figure 5, anatase and rutile were both formed after annealing. At the macroscopic level, rutile generally stands as thermodynamically stable structure of titania. However, when the particle size decreases below 14 nm, anatase seems to be more stable than rutile. This may explain why the anatase phase is dominant in mixed phase in our work, as SEM, TEM, and XRD results show that most particle size is well below 14 nm, in addition to a small number of particles.

3.4. Photocatalytic Activity. Figure 7 shows the photocatalytic activity of different samples. The first sample is pure TiO_2, the third sample is Ag/TiO_2, and the forth sample is rutile nanoparticles. The crystal structure of rutile is demonstrated in Figure 6 and the average particles size is about 15 nm estimated by Scherrer formula. In order to reveal the role of Ag nanoparticles more clearly, titania with less deposited Ag nanoparticles was fabricated as a reference sample by tuning irradiation time of laser ablation. This silver deposited titania is marked as $Ag/TiO_2{}'$.

Under UV irradiation, the rutile has a slightly higher degradation percent than that of pure TiO_2 as shown in Figure 7. When Ag nanoparticles are deposited into TiO_2, the degradation rate has been significantly increased. In particular, Ag/TiO_2 shows 41.5% and 40.7% degradation rate growth compared to pure TiO_2 and rutile. Thus, it can be seen that the photocatalytic activity of TiO_2 for the oxidative degradation

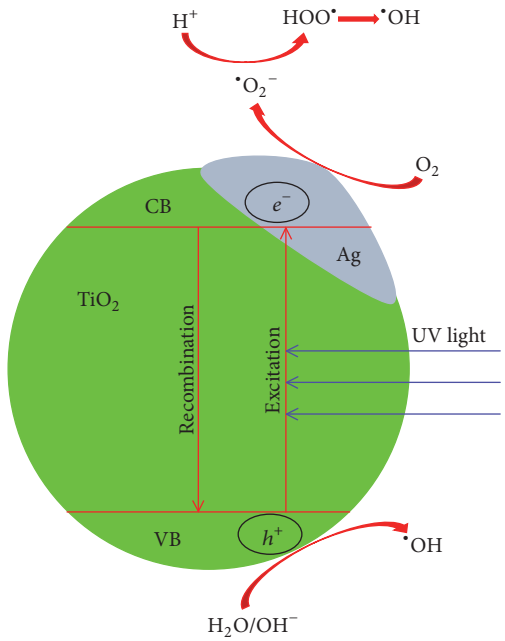

FIGURE 8: Photocatalytic pathways for the MB photodegradation on Ag/TiO_2 particles.

of MB is enhanced by coupling with Ag nanoparticles. The enhanced ability of MB degradation in the Ag/TiO_2 composite may be attributed to cooperative effect of Ag deposition according to the following three mechanisms. (i) More MB molecules are adsorbed on the surface of Ag/TiO_2′ and Ag/TiO_2 than that of TiO_2. It can facilitate the sensitized MB to the conduction band and then increase the possibility of electron transfer to O_2. (ii) Captured energy from input light source can excite the surface plasmon resonance of Ag nanoparticles, promoting the surface and interfacial electron transfer, enhancing electron-hole separation [42]. (iii) Ag nanoparticles act as electron traps in TiO_2 which would reduce the electron-hole recombination rate and enhance the subsequent transfer of the trapped electron to the adsorbed O_2 as electron acceptor [43].

As the LED light source with the wavelength of 365 nm was employed in this work, Ag surface plasmon resonance could not be excited by UV light. Hence, the mechanisms (i) and (ii) are not applicable in this work. Thus, only mechanism (iii) is feasible. A TiO_2-sensitization pathway for the MB photodegradation under UV light is demonstrated in Figure 8. The valence electrons of TiO_2 nanoparticles are excited to the conduction band by UV light. These electrons on the TiO_2 nanoparticles surface would be scavenged by the present molecular oxygen and then produce reactive oxygen radicals. In the meantime, the valence hole is trapped as the surface-bound $OH^•$ radicals on the oxidation of both OH^- groups and H_2O molecules on the surface. The generated materials could effectively degrade MB molecules. Consequently, the charge separation on TiO_2 is a vitally important factor to affect the result of the MB photodegradation in TiO_2. When Ag nanoparticles are deposited on the TiO_2 surface, because Fermi level of TiO_2 is higher than that of Ag, the electrons can transfer from TiO_2 to Ag until both Fermi levels are the same. It causes the Schottky barriers at Ag/TiO_2 contact region and the Ag nanoparticles acting as electron traps, leading to the reduction of electron-hole recombination in the photocatalytic process.

4. Conclusions

Pulsed laser ablation is successfully employed to continuously fabricate Ag/TiO_2 composite nanoparticles which are used in photocatalytic degradation. The Ag nanoparticles are found to enhance the TiO_2 photocatalytic activity. The MB photodegradation was carried out in TiO_2, Ag/TiO_2, and rutile in the same photo-reaction condition. Compared with the pure TiO_2 and rutile, the Ag/TiO_2 shows an obvious enhancement in the MB photodegradation under UV light irradiation, which could be attributed to the Ag nanoparticles by acting as electron traps.

Conflicts of Interest

The authors declare that they have no conflicts of interest.

Acknowledgments

This work was supported by the National Natural Science Foundation of China [Grant no. 61605162]; National Basic Research Program of China [Grant no. 2013CBA01703]; the Natural Science Foundation of Fujian Province of China [Grant no. 2017J05106]; the National Natural Science Foundation of China [Grant no. U1609209]; Zhejiang Provincial Key Laboratory of Laser Processing Robot/Key Laboratory of Laser Precision Processing & Detection [Grant no. lzsy-17]; and the Fundamental Research Funds for the Central Universities [Grant no. JB2016004].

References

[1] J. F. Budarz, A. Turolla, A. F. Piasecki, J.-Y. Bottero, M. Antonelli, and M. R. Wiesner, "Influence of aqueous inorganic anions on the reactivity of nanoparticles in TiO_2 photocatalysis," *Langmuir*, vol. 33, no. 11, pp. 2770–2779, 2017.

[2] M. C. Long, J. Brame, F. Qin, J. M. Bao, Q. L. Li, and P. J. J. Alvarez, "Phosphate changes effect of humic acids on TiO2 photocatalysis: from inhibition to mitigation of electron-hole recombination," *Environmental Science and Technology*, vol. 51, pp. 514–521, 2017.

[3] J. J. M. Vequizo, H. Matsunaga, T. Ishiku, S. Kamimura, T. Ohno, and A. Yamakata, "Trapping-induced enhancement of photocatalytic activity on brookite TiO_2 powders: comparison with anatase and rutile TiO_2 powders," *ACS Catalysis*, vol. 7, pp. 2644–2651, 2017.

[4] J. H. Lee, M. Kang, S.-J. Choung et al., "The preparation of TiO_2 nanometer photocatalyst film by a hydrothermal method and its sterilization performance for Giardia lamblia," *Water Research*, vol. 38, no. 3, pp. 713–719, 2004.

[5] R. W. Matthews, "Solar-electric water purification using photocatalytic oxidation with TiO_2 as a stationary phase," *Solar Energy*, vol. 38, no. 6, pp. 405–413, 1987.

[6] B. S. Necula, L. E. Fratila-Apachitei, S. A. J. Zaat, I. Apachitei, and J. Duszczyk, "In vitro antibacterial activity of porous TiO_2-Ag composite layers against methicillin-resistant Staphylococcus aureus," *Acta Biomaterialia*, vol. 5, no. 9, pp. 3573–3580, 2009.

[7] N. A. Ramos-Delgado, M. A. Gracia-Pinilla, L. Maya-Treviño, L. Hinojosa-Reyes, J. L. Guzman-Mar, and A. Hernández-Ramírez, "Solar photocatalytic activity of TiO_2 modified with WO_3 on the degradation of an organophosphorus pesticide," *Journal of Hazardous Materials*, vol. 263, pp. 36–44, 2013.

[8] O. Akhavan, "Lasting antibacterial activities of Ag-TiO_2/Ag/a-TiO_2 nanocomposite thin film photocatalysts under solar light irradiation," *Journal of Colloid and Interface Science*, vol. 336, no. 1, pp. 117–124, 2009.

[9] E. Szabó-Bárdos, H. Czili, and A. Horváth, "Photocatalytic oxidation of oxalic acid enhanced by silver deposition on a TiO_2 surface," *Journal of Photochemistry and Photobiology A: Chemistry*, vol. 154, no. 2-3, pp. 195–201, 2003.

[10] R. Peng, J. Baltrusaitis, C.-M. Wu, and R. T. Koodali, "Pd-Ti-MCM-48 cubic mesoporous materials for solar simulated hydrogen evolution," *International Journal of Hydrogen Energy*, vol. 40, no. 2, pp. 905–918, 2015.

[11] D.-I. Won, J.-S. Lee, J.-M. Ji et al., "Highly robust hybrid photocatalyst for carbon dioxide reduction: tuning and optimization of catalytic activities of Dye/TiO_2/Re(I) organic-inorganic ternary systems," *Journal of the American Chemical Society*, vol. 137, no. 42, pp. 13679–13690, 2015.

[12] K. Wilke and H. D. Breuer, "The influence of transition metal doping on the physical and photocatalytic properties of titania," *Journal of Photochemistry and Photobiology A: Chemistry*, vol. 121, no. 1, pp. 49–53, 1999.

[13] M. Anpo and M. Takeuchi, "The design and development of highly reactive titanium oxide photocatalysts operating under visible light irradiation," *Journal of Catalysis*, vol. 216, no. 1-2, pp. 505–516, 2003.

[14] A. Hamad, L. Li, Z. Liu, X. L. Zhong, H. Liu, and T. Wang, "Generation of silver titania nanoparticles from an Ag-Ti alloy via picosecond laser ablation and their antibacterial activities," *RSC Advances*, vol. 5, no. 89, pp. 72981–72994, 2015.

[15] Q. Lu, Z. Lu, Y. Lu et al., "Photocatalytic synthesis and photovoltaic application of Ag-TiO_2 nanorod composites," *Nano Letters*, vol. 13, no. 11, pp. 5698–5702, 2013.

[16] H. Tada, K. Teranishi, Y.-I. Inubushi, and S. Ito, "TiO_2 photocatalytic reduction of bis(2-dipyridyl)disulfide to 2-mercaptopyridine by H_2O: Incorporation effect of nanometer-sized Ag particles," *Chemical Communications*, no. 21, pp. 2345-2346, 1998.

[17] X. Zhou, G. Liu, J. Yu, and W. Fan, "Surface plasmon resonance-mediated photocatalysis by noble metal-based composites under visible light," *Journal of Materials Chemistry*, vol. 22, no. 40, pp. 21337–21354, 2012.

[18] Y. Yang, G. Zhang, and W. Xu, "Facile synthesis and photocatalytic properties of AgAgClTiO_2/rectorite composite," *Journal of Colloid and Interface Science*, vol. 376, no. 1, pp. 217–223, 2012.

[19] M. Pirhashemi and A. Habibi-Yangjeh, "Ultrasonic-assisted preparation of plasmonic ZnO/Ag/Ag2WO4 nanocomposites with high visible-light photocatalytic performance for degradation of organic pollutants," *Journal of Colloid and Interface Science*, vol. 491, pp. 216–229, 2017.

[20] A. Akhundi and A. Habibi-Yangjeh, "High performance magnetically recoverable g-C3N4/Fe3O4/Ag/Ag2SO3 plasmonic photocatalyst for enhanced photocatalytic degradation of water pollutants," *Advanced Powder Technology*, vol. 28, no. 2, pp. 565–574, 2017.

[21] A. Sclafani and J.-M. Herrmann, "Influence of metallic silver and of platinum-silver bimetallic deposits on the photocatalytic activity of titania (anatase and rutile) in organic and aqueous media," *Journal of Photochemistry and Photobiology A: Chemistry*, vol. 113, no. 2, pp. 181–188, 1998.

[22] V. Vamathevan, R. Amal, D. Beydoun, G. Low, and S. McEvoy, "Photocatalytic oxidation of organics in water using pure and silver-modified titanium dioxide particles," *Journal of Photochemistry and Photobiology A: Chemistry*, vol. 148, no. 1-3, pp. 233–245, 2002.

[23] F. Zhang, R. Jin, J. Chen et al., "High photocatalytic activity and selectivity for nitrogen in nitrate reduction on Ag/TiO_2 catalyst with fine silver clusters," *Journal of Catalysis*, vol. 232, no. 2, pp. 424–431, 2005.

[24] C. H. Liu, M. H. Hong, Y. Zhou, G. X. Chen, M. M. Saw, and A. T. S. Hor, "Synthesis and characterization of Ag deposited TiO_2 particles by laser ablation in water," *Physica Scripta*, vol. 2007, p. 326, 2007.

[25] G. X. Chen, M. H. Hong, Q. He et al., "Formation, structure and nonlinear optical properties of carbon nanoparticles synthesized by pulsed laser ablation," *Applied Physics A: Materials Science & Processing*, vol. 79, no. 4-6, pp. 1079–1082, 2004.

[26] G. X. Chen, M. H. Hong, T. C. Chong, H. I. Elim, G. H. Ma, and W. Ji, "Preparation of carbon nanoparticles with strong optical limiting properties by laser ablation in water," *Journal of Applied Physics*, vol. 95, no. 3, pp. 1455–1459, 2004.

[27] D. Zhang, B. Gökce, and S. Barcikowski, "Laser synthesis and processing of colloids: fundamentals and applications," *Chemical Reviews*, vol. 117, no. 5, pp. 3990–4103, 2017.

[28] Z. B. Zhang, C. C. Wang, R. Zakaria, and J. Y. Ying, "Role of particle size in nanocrystalline TiO_2-based photocatalysts," *The Journal of Physical Chemistry B*, vol. 102, pp. 10871–10878, 1998.

[29] N. Xu, Z. Shi, Y. Fan, J. Dong, J. Shi, and M. Z. C. Hu, "Effects of particle size of TiO_2 on photocatalytic degradation of methylene blue in aqueous suspensions," *Industrial & Engineering Chemistry Research*, vol. 38, no. 2, pp. 373–379, 1999.

[30] X. Chen, D. Zhao, K. Liu et al., "Laser-modified black titanium oxide nanospheres and their photocatalytic activities under visible light," *ACS Applied Materials and Interfaces*, vol. 7, no. 29, pp. 16070–16077, 2015.

[31] T. Sasaki, Y. Shimizu, and N. Koshizaki, "Preparation of metal oxide-based nanomaterials using nanosecond pulsed laser ablation in liquids," *Journal of Photochemistry and Photobiology A: Chemistry*, vol. 182, no. 3, pp. 335–341, 2006.

[32] F. Mafuné, J.-Y. Kohno, Y. Takeda, and T. Kondow, "Formation of stable platinum nanoparticles by laser ablation in water," *The Journal of Physical Chemistry B*, vol. 107, no. 18, pp. 4218–4223, 2003.

[33] V. Amendola and M. Meneghetti, "What controls the composition and the structure of nanomaterials generated by laser ablation in liquid solution?" *Physical Chemistry Chemical Physics*, vol. 15, no. 9, pp. 3027–3046, 2013.

[34] F. Barreca, N. Acacia, E. Barletta, D. Spadaro, G. Currò, and F. Neri, "Small size TiO_2 nanoparticles prepared by laser ablation in water," *Applied Surface Science*, vol. 256, no. 21, pp. 6408–6412, 2010.

[35] D. Chu, A. Younis, and S. Li, "Direct growth of TiO_2 nanotubes on transparent substrates and their resistive switching characteristics," *Journal of Physics D: Applied Physics*, vol. 45, no. 35, Article ID 355306, 2012.

[36] P. Liu, W. Cai, M. Fang et al., "Room temperature synthesized rutile TiO_2 nanoparticles induced by laser ablation in liquid and their photocatalytic activity," *Nanotechnology*, vol. 20, no. 28, Article ID 285707, 2009.

[37] M. I. Litter, "Heterogeneous photocatalysis: Transition metal ions in photocatalytic systems," *Applied Catalysis B: Environmental*, vol. 23, no. 2-3, pp. 89–114, 1999.

[38] Q. Zhang, L. Gao, and J. Guo, "Effects of calcination on the photocatalytic properties of nanosized TiO_2 powders prepared by $TiCl_4$ hydrolysis," *Applied Catalysis B: Environmental*, vol. 26, no. 3, pp. 207–215, 2000.

[39] C. C. Wang and J. Y. Ying, "Sol-gel synthesis and hydrothermal processing of anatase and rutile titania nanocrystals," *Chemistry of Materials*, vol. 11, no. 11, pp. 3113–3120, 1999.

[40] R. A. Spurr, "Quantitative analysis of anatase-rutile mixtures with an X-ray diffractometer," *Analytical Chemistry*, vol. 29, no. 5, pp. 760–762, 1957.

[41] S. Bégin-Colin, A. Gadalla, G. Le Caër et al., "On the origin of the decay of the photocatalytic activity of TiO_2 powders ground at high energy," *The Journal of Physical Chemistry C*, vol. 113, no. 38, pp. 16589–16602, 2009.

[42] G. Lassaletta, A. R. González-Elipe, A. Justo et al., "Thermal and photochemical methods for the preparation of thin films of cermet materials," *Journal of Materials Science*, vol. 31, no. 9, pp. 2325–2332, 1996.

[43] J.-M. Herrmann, J. Disdier, and P. Pichat, "Oxygen species ionosorbed on powder photocatalyst oxides from room-temperature photoconductivity as a function of oxygen pressure," *Journal of the Chemical Society, Faraday Transactions 1: Physical Chemistry in Condensed Phases*, vol. 77, no. 11, pp. 2815–2826, 1981.